




THEORETICAL ANALYSIS OF SOLAR THERMOELECTRIC GENERATORS INTEGRATED WITH RADIATIVE COOLER

*Aminu YUSUF 


Istanbul University-Cerrahpaşa, Engineering Sciences Department, Istanbul, TÜRKİYE
aminu.yusuf@iuc.edu.tr

Highlights

- Solar thermoelectric generator is passively cooled by a radiative cooler.
- Ambient temperature has a positive influence on the cooling power.
- Wind speed has a negative influence on the cooling power.
- An increase in the relative humidity reduces the generator's output power.



THEORETICAL ANALYSIS OF SOLAR THERMOELECTRIC GENERATORS INTEGRATED WITH RADIATIVE COOLER

*Aminu YUSUF 

Istanbul University-Cerrahpaşa, Engineering Sciences Department, Istanbul, TÜRKİYE
aminu.yusuf@iuc.edu.tr

(Received: 07.08.2023; Accepted in Revised Form: 21.11.2023)

ABSTRACT: A comprehensive analysis of solar thermoelectric generators integrated with radiative cooling technology (STEG-RC) is presented in this study. Basically, the STEG-RC operates outdoors; therefore, the effects of various weather parameters on the output performance of the STEG-RC are determined. The results reveal that the most efficient way of enhancing the output performance of the STEG-RC is by concentrating solar energy. The radiative cooling power increases linearly with the ambient temperature achieving the maximum cooling power of 135 W/m² and 232 W/m² at solar concentration ratios of $C = 1$ and $C = 5$, respectively. The maximum output power of 1.5 mW and 459.6 mW at the optimum wind speeds of 3 m/s and 2 m/s are obtained for $C = 1$ and $C = 5$, respectively. There were no significant changes in the power output and radiative cooling power when relative humidity was varied. The cooling power is linearly proportional to solar irradiance for both concentrated and unconcentrated cases.

Keywords: *Cooling power, Passive cooling, Radiative cooling, Renewable energy, Thermoelectric generator*

1. INTRODUCTION

The high cost of fossil fuels and the increase in the greenhouse effect are some of the reasons that necessitate the search for other alternative energy sources [1]. Solar energy is the most abundant free energy on earth, and if harnessed efficiently, the greenhouse effect can be alleviated. A thermoelectric generator (TEG) is one of the energy harvesters that converts thermal energy directly into electrical energy [2]–[5]. A selective absorber exposed under the sun can absorb solar radiation energy and convert it into thermal energy for TEG, leading to a solar TEG (STEG). A TEG does not only operate in the daytime but also at nighttime; it has no moving parts, no noise, or vibration [6]. In the last decade, research interest in solar TEGs (STEGs) has increased significantly; this is to ensure optimum utilization of the solar spectrum. For example, Bekele and Ancha [7] proposed a solar concentrator integrated with Stirling and TEG to power a water pump for irrigation purposes. The TEG achieved a maximum output power of 5.2 W and an energy conversion efficiency of 2.78%. Although the system is capable of powering a water pump, the authors suggested that the system needs further optimization. Liu et al. [8] developed a solar selective absorber (CuCrMnCoAlN-based) to enhance the performance of a STEG. The as-synthesized solar selective absorber has an absorptivity of 95.2% and emissivity of 10.9%. Integrating the solar absorber with a commercial STEG results in an output power of 1.99 mW. Sun et al. [9] developed a transient model of STEG using a three-dimensional numerical model. For a solar concentration ratio of 150, the annual energy production of the developed model was 49.79 kW/h, and the cost-recovery cycle was found to be 1.61 years. Alobaid et al. [10] compared the thermo-mechanical performance of frustrum-shaped, trapezoidal-shaped, and rectangular-shaped thermoelectric legs using a three-dimensional finite element model. The study also reveals that the output performance prediction using a neural network is 702 times faster than the performance prediction using the numerical analysis method.

STEGs like photovoltaics operate only during the day; however, nighttime operation can be achieved by coupling phase change material (PCM) on the hot side of the STEG. The PCM absorbs and stores a large amount of solar energy until phase transformation is completed [11], [12]. Thus, the PCM provides

*Corresponding Author: Aminu YUSUF, aminu.yusuf@iuc.edu.tr

stable and uniform thermal energy to the STEG during and after the sunshine hours. Since most of the commercial PCMs have poor heat transfer due to low thermal conductivity, the thermal performance can be increased by mixing metal particles with the PCM [13]. PCM can also serve as a heat sink when integrated on the cold side of the STEG [14]. In this manner, the PCM absorbs and stores the heat from the cold side of the STEG.

Using a different approach, radiative cooling (RC) can be employed to achieve 24-hour power generation of the STEG [15]. Radiative cooling passively cools the cold side temperature of the STEG in the daytime, nighttime, and a combination of the two [16]. The RC reflects the solar energy in the daytime and emits radiation at nighttime through a sky window (wavelength between 8 – 13 μm) [17]. An ideal RC for 24-hour operation should have high solar energy reflectivity in the daytime and high emissivity at nighttime. However, an ideal radiative cooling material has not been found yet. In the past, radiative cooling technology has been used in the cooling of photovoltaics, buildings, power plant condensers, and dew water harvesting [18]. The radiative cooling technology is capable of lowering the temperature of a surface to 14 $^{\circ}\text{C}$ and 12 $^{\circ}\text{C}$ below the ambient temperature in laboratory and outdoor tests, respectively [19]. This indicates that RC can significantly enhance the output performance of a STEG. To validate that, Liu et al. [20] developed a model of TEG integrated with a heat sink – RC (TEG-HS-RC) and another model consisting of only TEG-HS. The analysis revealed that the TEG-HS-RC model is superior to the TEG-RH model by about 32%.

Although STEG has been extensively studied, the integration of radiative cooling with the STEG has only been recently considered; hence, many research gaps need to be addressed. Most importantly, the STEG-RC operates outdoors; therefore, its operation can be influenced by weather parameters. In line with that, this study is carried out to determine the influence of ambient temperature, wind speed, relative humidity, and solar irradiance on the output performance of the STEG-RC. Additionally, the influence of concentrating solar energy on the operation of the STEG-RC is investigated.

2. MATERIAL AND METHODS

The model presented in Figure 1 consists of a solar concentrator (reflective mirror), an STEG coated with a selective absorber on the hot side, and a radiative cooler on the cold side. Solar energy is concentrated on the hot side of the STEG where the energy is absorbed by the selective absorber. On the hot side, both radiation and convection losses occur, and eventually, the STEG converts part of the absorbed energy into electrical power while the rest is transferred to the cold side via conduction. The balanced energy transfer process is mathematically given as:

$$A_{TE}CG\tau_g\alpha_{sa} = A_{TE}\varepsilon\sigma_s(T_h^4 - T_{sky}^4) + A_{TE}h_{conv}(T_h - T_a) + \frac{N[S(T_h - T_c)]^2}{4R} + \frac{T_c - T_{rc}}{R_{c-rc}} \quad (1)$$

where the term on the left-hand side is the energy input, the first and second terms on the right-hand side are the radiation and convection losses, and the third and fourth terms are the maximum output power and energy transferred by conduction. C and G are the concentration ratio and solar irradiance, τ_g and α_{sa} are the transmissivity of glass and absorptivity of the selective absorber, ε and σ_s are the emissivity of the hot side and Stefan Boltzmann constant, N is the number of thermocouples, T_{sky} is the temperature of the sky, T_h and T_c are the temperatures of hot and cold sides, T_{rc} and R_{c-rc} are the temperature of the radiative cooler and the thermal resistance between the cold side and the radiative cooler, S , A_{TE} , R are the Seebeck coefficient, surface area, and internal resistance of the STEG, respectively. A windshield cover is not integrated into this model; therefore, the convective heat transfer coefficient can be given as [21]:

$$h_{conv} = 8.3 + 2.5v \quad (2)$$

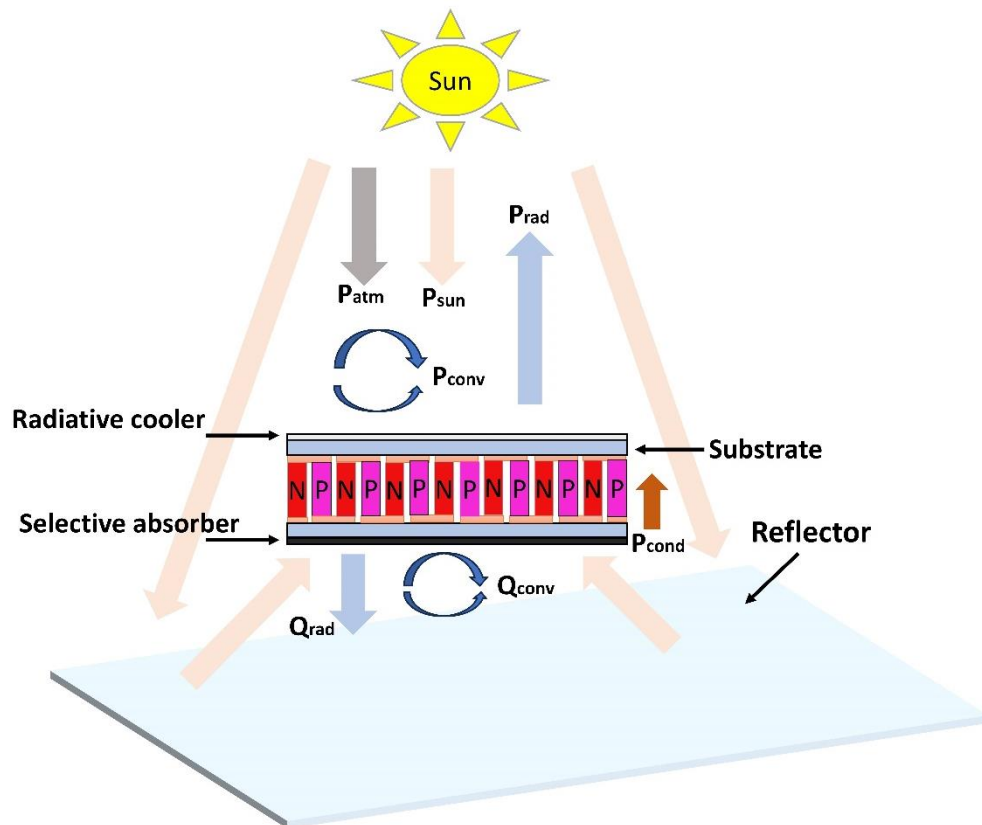


Figure 1. Solar-concentrated thermoelectric generator

The density of the energy transferred by conduction from the hot side to the cold is the same as the density of the energy transferred from the cold side to the radiative cooler and is given as:

$$P_{cond} = \frac{T_h - T_c}{A_{TE} R_{KTE}} = \frac{T_c - T_{rc}}{A_{TE} R_{c-rc}} \quad (3)$$

At a steady state, the sum of the energy radiated by the radiative cooler and the convection loss should be equal to the sum of the energy absorbed by the radiative cooler, atmospheric energy absorption by the radiative cooler, and the energy absorbed through the conduction:

$$P_{rad} + P_{conv} = P_{sun} + P_{atm} + P_{cond} \quad (4)$$

The energy radiated by the radiative cooler also known as the cooling power is [22]:

$$P_{rad}(T_{rc}) = \int_0^{2\pi} d\varphi \int_0^{\frac{\pi}{2}} \sin\theta \cos\theta d\theta \int_0^{\infty} I_{bb}(\lambda, T_{rc}) \varepsilon_{rc}(\lambda, \theta, \varphi) d\lambda \quad (5)$$

where φ is the solid angle, θ is the zenith angle, λ is the wavelength, $\varepsilon_{rc}(\theta, \lambda)$ is the emissivity of radiative cooler, the spectral radiance of a blackbody $I_{bb}(\lambda, T_{rc})$ at temperature T_{rc} is defined as [23]:

$$I_{bb}(\lambda, T_{rc}) = \frac{2hc^2}{\lambda^5 \left(e^{\frac{hc}{\lambda k T_{rc}}} - 1 \right)} \quad (6)$$

where Planck's constant $h = 6.626 \times 10^{-34}$ J s, Boltzmann constant $k = 1.381 \times 10^{-23}$ J/K, speed of light $c = 2.998 \times 10^8$ m/s.

The convection density is thus given as:

$$P_{conv} = h_{conv}(T_{rc} - T_a) \quad (7)$$

The sun energy absorbed by the radiative cooler can be calculated from:

$$P_{sun} = \int_0^{\infty} I_{solar}(\lambda) \varepsilon_{rc}(\lambda) \cos\theta d\lambda \quad (8)$$

where $I_{solar}(\lambda)$ is the solar spectral irradiation intensity.

The atmospheric power absorbed by the radiative cooler is given as:

$$P_{atm}(T_a) = \int_0^{\infty} \int_0^{2\pi} \int_0^{\frac{\pi}{2}} \alpha_{rc}(\lambda, \theta, \varphi) I_{\lambda,b}(T_a, \lambda) \varepsilon_{atm}(\lambda, \theta) \sin\theta \cos\theta d\lambda d\varphi d\theta \quad (9)$$

where T_a is the ambient temperature, $I_{\lambda,b}(T_a, \lambda)$ is the spectral irradiance of a blackbody at the ambient temperature, $\alpha_{rc}(\lambda, \theta, \varphi)$ is the absorptivity of the radiative cooler, $\varepsilon_{atm}(\lambda, \theta)$ is the atmospheric emissivity given as [24]:

$$\varepsilon_{atm} = 0.727 + 0.006T_{dew} \quad (10)$$

where T_{dew} (°C) is the dew point temperature, which is calculated from:

$$T_{dew} = \frac{243.12 \left[\ln\left(\frac{RH}{100}\right) + \frac{17.62T_a}{243.12 + T_a} \right]}{17.62 - \left[\ln\left(\frac{RH}{100}\right) + \frac{17.62T_a}{243.12 + T_a} \right]} \quad (11)$$

where the unit of T_a in Eq. 11 is °C. The relationship between the temperature of the sky and the emissivity of the sky is:

$$T_{sky} = \varepsilon_{atm}^4 T_a \quad (12)$$

The thermal resistance between the cold side and the radiative cooler is:

$$R_c = \frac{L_c}{K_c A_c} \quad (13)$$

where L_c is the thickness of the cold side, K_c and A_c are the thermal conductivity and surface area of the cold side.

The internal resistance of a unicouple STEG, which is used to calculate the output power is:

$$R = \frac{L_p}{\sigma_p A_p} + \frac{L_n}{\sigma_n A_n} \quad (14)$$

where L is the length of the TE leg, A is the cross-sectional area of the TE legs, σ is the electrical conductivity, k is the thermal conductivity, subscripts p and n represent the type of TE materials.

The thermal resistance of the STEG is one of the factors that affects the temperature gradient of the STEG. The temperature gradient increases with an increase in the thermal resistance. As given in equation 15, the longer the leg length, the higher the thermal resistance.

$$R_{KTE} = \frac{L}{N(A_n k_n + A_p k_p)} \quad (15)$$

Herein, the adopted radiative cooler (TiO₂ + SiO₂) has a reflectivity in the solar spectrum of 90.7% and an emittance of 90.11% in the sky window [25]. Likewise, Al₂O₃-filled nanocavity photonic crystal is the adopted selective absorber with an average solar absorptivity of 0.8 in the solar spectrum [26]. The

transport properties of the TE materials are given in Table 1 and the parameters of STEG are given in Table 2.

Table 1. Thermoelectric properties of the chalcogenides [27]

Property	Expression
S_p	$(1.023898 - 7.301 \times 10^{-3} T + 2.22834 \times 10^{-5} T^2 - 2.24407 \times 10^{-8} T^3) \times 10^{-3}$ V/K
S_n	$(-9.54589 \times 10^{-4} + 6.203 \times 10^{-6} T - 1.77163 \times 10^{-8} T^2 + 1.68178 \times 10^{-11} T^3)$ V/K
σ_p	$(1.60117 \times 10^{-5} - 0.01853 \times 10^{-5} T + 7.77051 \times 10^{-10} T^2 - 7.75456 \times 10^{-13} T^3)$ S/m
σ_n	$(2.11951 \times 10^{-5} - 1.715 \times 10^{-7} T + 6.09155 \times 10^{-10} T^2 - 6.04782 \times 10^{-14} T^3)$ S/m
k_p	$(8.726 - 0.05011 T + 1.03491 \times 10^{-4} T^2 - 5.82609 \times 10^{-8} T^3)$ W/(m K)
k_n	$(5.09531 - 0.02057 T + 2.81722 \times 10^{-5} T^2 + 3.76869 \times 10^{-9} T^3)$ W/(m K)

Table 2. Parameters of the STEG

Parameter	value
TE leg	$1 \times 1 \times 1.5$ mm ³
Number of TE couples	127
Thickness of Al ₂ O ₃ substrate	0.5 mm ³
Thickness of copper electrode	50 μm
Thickness of radiative cooler	10 μm
Thickness of selective absorber	10 μm
Thickness of glass cover	1 mm
Module size	$40 \times 40 \times 2.6$ mm ³

The above equations are solved in MATLAB to determine the cooling performance of the radiative cooler and the output power of the STEG. Unlike stated otherwise, the ambient temperature of 23 °C, relative humidity of 30%, solar radiation of 1000 W/m², and wind speed of 2 m/s are used.

3. RESULTS AND DISCUSSION

To determine the effect of solar concentration on both the performance of the radiative cooler and the STEG, the performance of concentrated ($C = 5$) and unconcentrated ($C = 1$) STEGs is investigated. The operation of both the radiative cooler and STEG strongly depends on weather parameters such as ambient temperature, relative humidity (RH), wind speed, and solar irradiance. The influence of these parameters, one at a time, is parametrically investigated.

3.1. Influence of ambient temperature on the output performance of the STEG-RC

As shown in Figure 2, the ambient temperature is varied from 5 °C to 45 °C to cover four weather seasons of a typical city in the Mediterranean region (Antalya, Türkiye). Figure 2a presents the hot and cold side temperatures of the STEG and the temperature of the radiative cooler at $C = 1$. The temperatures monotonically increase with the increase in the ambient temperature. The temperature gradient of the STEG decreases with the increase in the ambient temperature, and at a particular point, the temperature gradient approaches zero. The temperatures of the cold side and the radiative cooling surface are almost identical because the thermal resistance between the two surfaces is very low. Figure 2b presents the output power of the unconcentrated STEG and the radiative cooling power. The output power decreases with the increase in the ambient temperature due to the decrease in the temperature gradient. At $T_a = 5$ °C, the STEG generates an output power of 4 mW, while it reduces to zero at $T_a = 45$ °C. On the contrary, the radiative cooling power increases with the increase in the ambient temperature; this is mainly due to the increase in spectral radiance. At $T_a = 5$ °C, the RC cooling power is about zero, while it increases to 135 W/m² at $T_a = 45$ °C. Figure 2c presents the variation of the temperatures of the hot and cold sides and the temperature of the RC surface at $C = 5$. The temperatures increase with the

increase in the ambient temperature. Unlike in Figure 2a, where the temperature gradient approaches zero with the increase in the ambient temperature, a substantive temperature gradient is maintained in Figure 2c because the hot side kept increasing due to the concentration of solar energy. Figure 2d shows the output power of the STEG and the cooling power of RC at $C = 5$. The output power reduces from 510 mW to 30 mW, while the cooling power increases from 160 W/m² to 230 W/m² as the ambient temperature increases from 5 °C to 45 °C. These results indicate that the ambient temperature has a negative impact on the output performance of STEGs while it has a positive influence on the cooling performance of the RC. It can also be seen that by concentrating the solar energy by a ratio of 5, the cooling power is enhanced by 70.4%, and the output power is enhanced by more than 500%, indicating that concentrating the solar energy is the best way of enhancing the output performance of the STEG-RC.

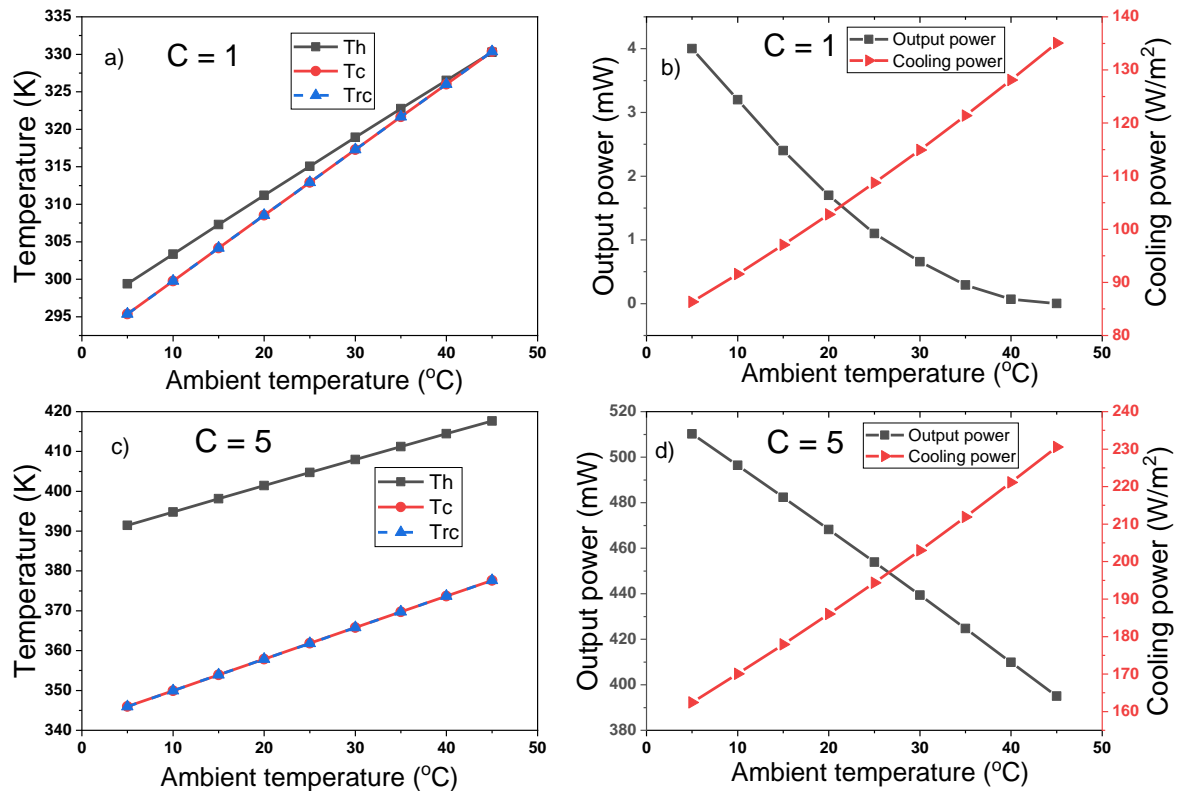


Figure 2. Effect of ambient temperature on a) temperatures of un-concentrated STEG, b) output power of un-concentrated STEG, c) temperatures of concentrated STEG, d) output power of concentrated STEG

3.2. Influence of relative humidity on the output performance of the STEG-RC

Figure 3 shows the effect of variations in relative humidity (RH) on the temperatures, output power, and cooling power for both concentrated and un-concentrated STEGs. As RH is varied from 10% to 90%, temperatures of both the STEG and RC slightly increase, as shown in Figure 3a. This result indicates that RH does not have much influence on the temperatures because its primary effect is on atmospheric emissivity through the dew point temperature. Figure 3b presents the output power of the STEG and the cooling power of the RC at $C = 1$. The output power reduces with the increase in RH from 10% to 60%, after which it remains almost stable at about 1.2 mW. The cooling power, on the other hand, shows only a slight increase over the range of RH variation. A maximum cooling power of 106.8 W/m² is achieved at RH = 90%. Figure 3c presents the variation of the temperatures of the STEG and RC at $C = 5$. Over the range of RH variation, the temperature of the hot side remains almost constant, while the temperatures

of the cold side and RC surface slightly increase. This means that the temperature gradient of the STEG decreases with the increase in RH, as can be understood from the output power in Figure 3d. The output power reduces by about 1.5%, while the cooling power increases by 0.84% as RH is increased from 10% to 90%. In summary, RH has an insignificant influence on the output performance of both the STEG and RC for the concentrated and unconcentrated cases.

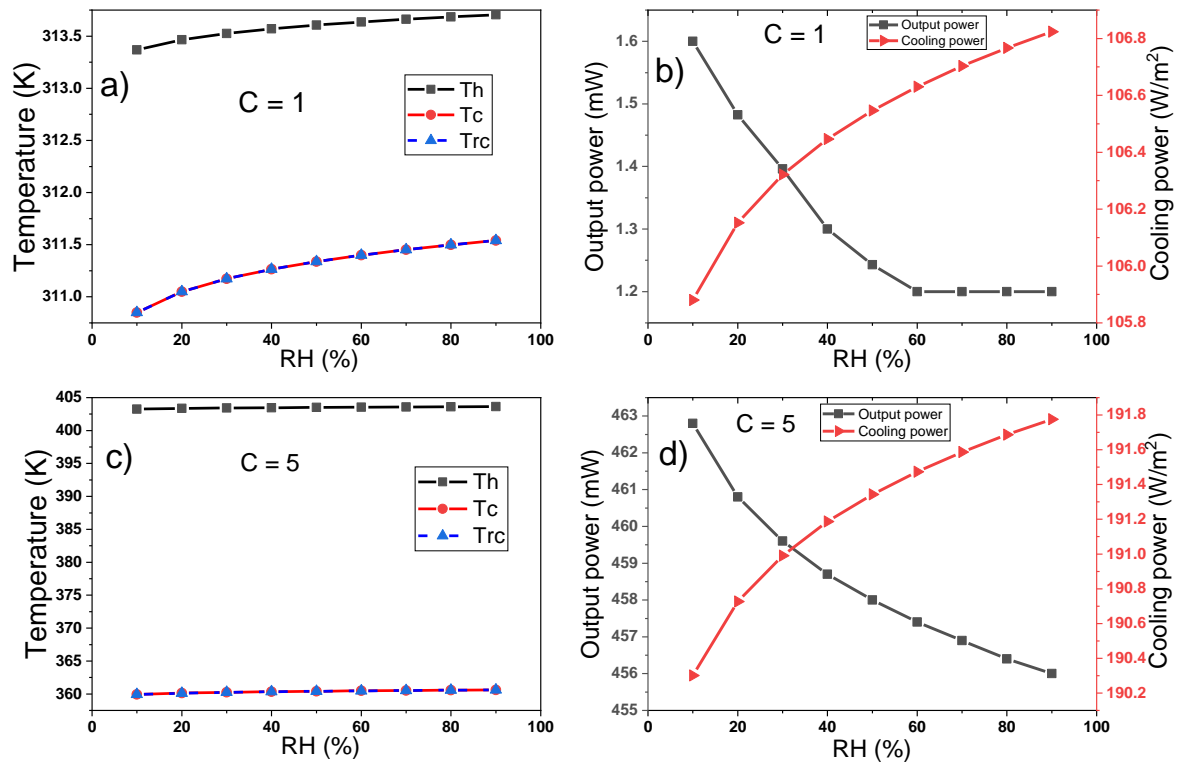


Figure 3. Effect of Relative humidity on a) temperatures of unconcentrated STEG, b) output power of unconcentrated STEG, c) temperatures of concentrated STEG, d) output power of concentrated STEG

3.3. Influence of wind speed on the output performance of the STEG-RC

The variation in temperatures of the unconcentrated STEG and RC surface with wind speed is shown in Figure 4a. Wind speed is associated with convection energy, and as wind speed increases, convection cooling also increases. Convection cooling affects both the hot and cold sides of the STEG, leading to a decrease in temperatures with an increase in wind speed. As wind speed is varied from 0 to 8 m/s, the temperature gradient increases from 1.9 to 2.5 K, resulting in the enhancement of output power as shown in Figure 4b. It can be observed that the output power starts decreasing once the optimum wind speed is exceeded. Determining the optimum wind speed is crucial to achieve the best output performance of a STEG. It should be noted that wind speed has a different impact on the cooling power of the RC. As per Equation 4, it is obvious to see that as wind speed increases, convection losses increase, which, in turn, decreases radiative cooling power. As wind speed increases from 0 to 8 m/s, the radiative cooling power decreases from 116 W/m² to 96 W/m², indicating that wind speed has a negative influence on cooling power. This is why a wind shield is usually employed in radiative cooling applications. Figure 4c presents the temperatures of the STEG and RC surface at C = 5. Figure 4c and Figure 4a show a similar trend, indicating that wind speed has the same effect on both concentrated and unconcentrated solar energy. Initially, the output power in Figure 4d increases and then decreases with the increase in wind speed. As mentioned earlier, the output power has a maximum value at the optimum wind speed. Herein, a maximum output power of 459.6 mW is achieved at the optimum wind speed of 2 m/s. As seen

in Figure 4b, the radiative cooling power in Figure 4d also decreases with the increase in wind speed for the same reasons mentioned earlier. As wind speed increases from 0 to 8 m/s, the radiative cooling power decreases from 255.7 W/m² to 128 W/m². In summary, wind speed has a negative effect on the radiative cooler; however, the optimum wind speed enhances the output power of a STEG.

Top of Form

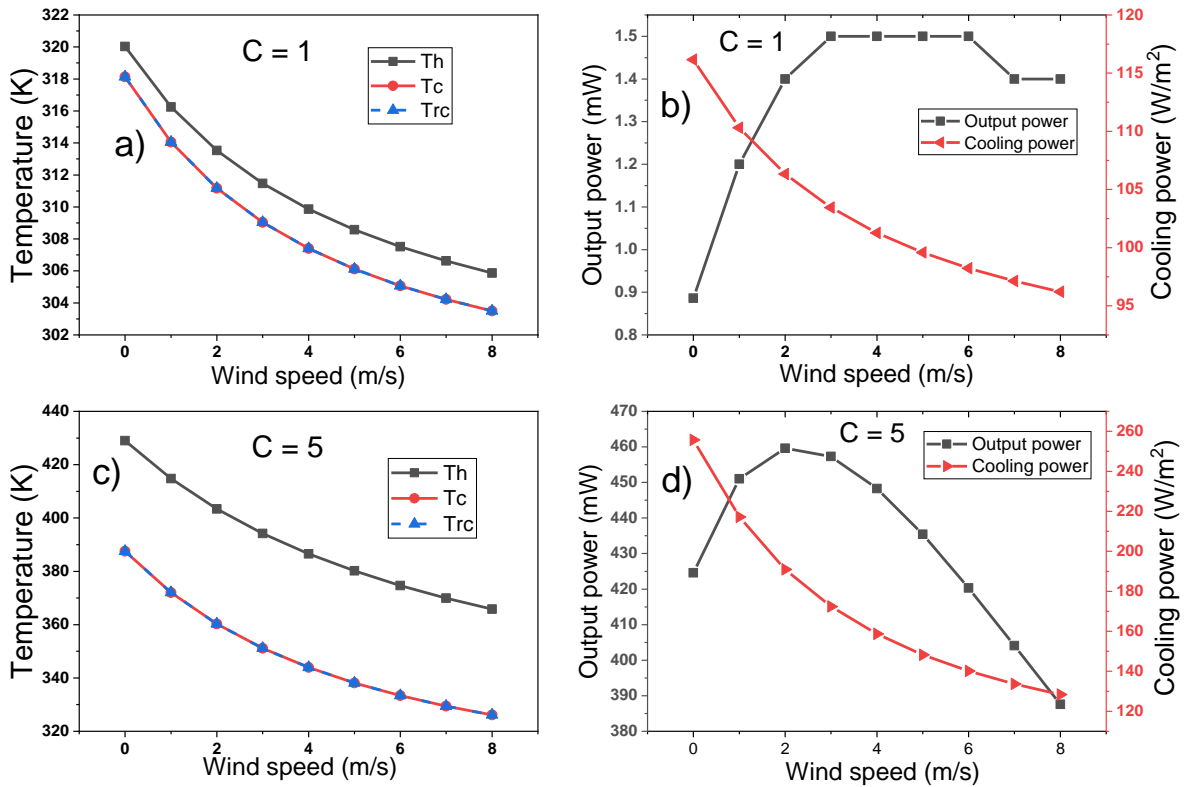


Figure 4. Effect of wind speed on a) temperatures of un-concentrated STEG, b) output power of un-concentrated STEG, c) temperatures of concentrated STEG, d) output power of concentrated STEG

3.4. Influence of solar irradiance on the output performance of the STEG-RC

Figure 5a presents the variation in temperatures of the STEG and RC surface with the variation in solar irradiance for the un-concentrated STEG. For a typical winter case (low solar irradiance), the surface temperature of the RC is higher than the temperature of the hot side. As solar irradiance increases from 100 W/m² to 700 W/m², the temperature of the hot side increases and becomes equal to the surface temperature of the RC. A further increase in solar irradiance leads to a further increase in the hot side temperature above the surface temperature of the RC. Figure 5b presents the output power of the STEG and the radiative cooling power of the RC at C = 1. Typically, a negative output power is expected when the temperature of the cold side is higher than that of the hot side due to the reverse current flow. However, in this analysis, absolute values of the output power are considered. Having said that, the output power decreases from 7.1 mW to 0 mW as solar irradiance increases from 100 W/m² to 700 W/m², after which the output power slightly increases. On the contrary, the radiative cooling power increases linearly with the increase in solar irradiance, in agreement with equation 5.

Figure 5c shows the temperatures of the STEG and the surface of RC with the variation of solar irradiance at C = 5. At a solar irradiance of 100 W/m², the temperatures have the same values; however, as solar irradiance increases, the hot side temperature becomes increasingly higher than the other temperatures. This is because the hot side receives 5-fold more energy than the cold side/RC. Figure 5d

presents the output power and the radiative cooling power at $C = 5$. The output power exponentially increases from 0 to 375 mW as solar irradiance increases from 100 W/m^2 to 900 W/m^2 . Similarly, the radiative cooling power increases linearly with solar irradiance. A maximum radiative cooling power of 180 W/m^2 is achieved at a solar irradiance of 900 W/m^2 . In summary, the unconcentrated STEG should not be operated at low solar irradiance to avoid reverse current flow. On the other hand, solar irradiance has a positive influence on the output power of the concentrated STEG. In both concentrated and unconcentrated cases, the radiative cooling power linearly increases with solar irradiance.

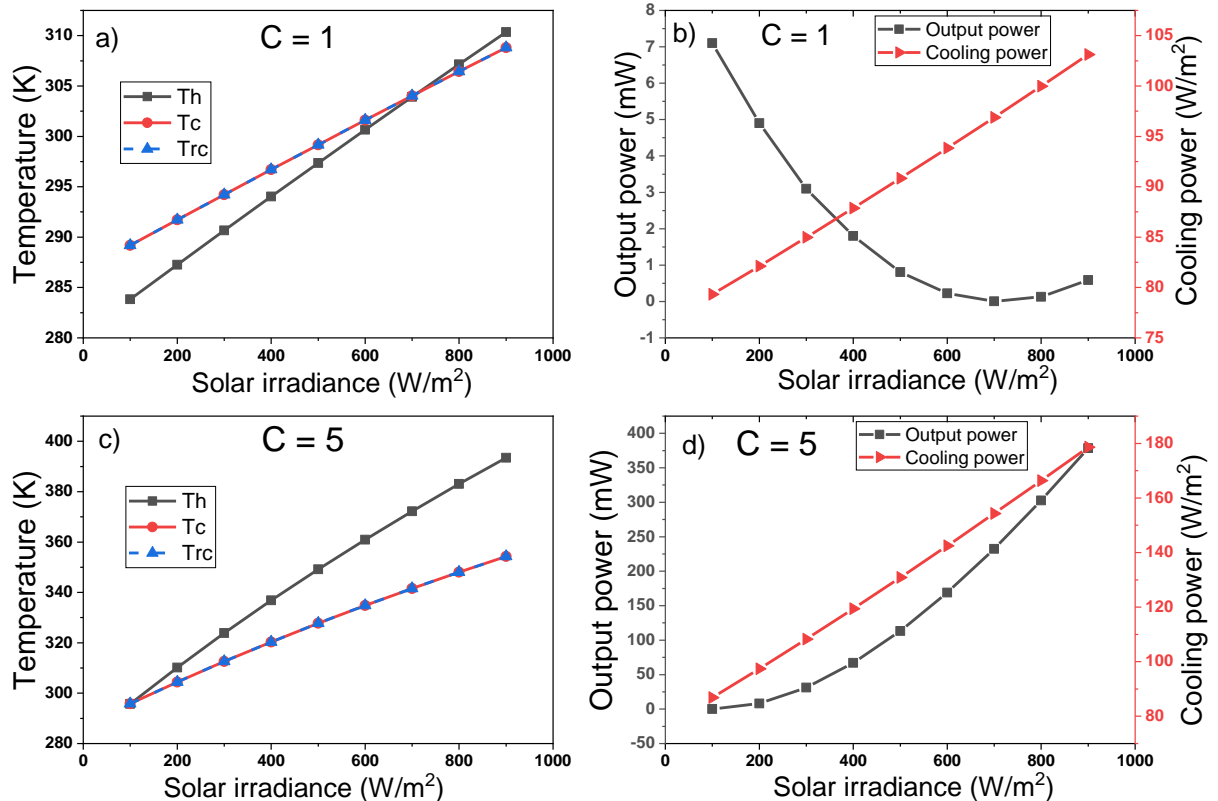


Figure 5. Effect of solar irradiance on a) temperatures of unconcentrated STEG, b) output power of unconcentrated STEG, c) temperatures of concentrated STEG, d) output power of concentrated STEG

The average cost of the unconcentrated and concentrated STEG-RC systems is about \$10 and \$50, respectively [28, 29]. A typical thermoelectric generator with chalcogenide TE materials operates in a temperature range of 300 – 500 K, which is the temperature range covered by this study. When operated properly, it can have a lifespan of 20 years or more [30], indicating its suitability for long-term energy harvesting applications. This also means a relatively competitive levelized cost of energy.

4. CONCLUSIONS

This study presents a steady-state theoretical analysis of STEG-RC for both concentrated and unconcentrated cases. Since the STEG-RC is expected to operate outdoors, the effect of weather parameters on the system's output performance needs to be determined. Based on the results presented, the main findings can be summarized as follows:

- Concentrating solar energy is the most effective way to enhance the output performance of STEG-RC.
- Ambient temperature negatively affects the output of the STEGs. At $C = 5$, the output power reduces from 510 mW to 395 mW when the ambient temperature increases from 5 $^{\circ}\text{C}$ to 45 $^{\circ}\text{C}$.

Similarly, the output power of the unconcentrated STEG reduces from 4 mW to 0 mW when the temperature changes from 5 °C to 45 °C.

- Relative humidity has an insignificant influence on both the output power and the radiative cooling power.
- An optimum wind speed is required to achieve the maximum output power of STEG-RC. The optimum wind speed is found to be 3 m/s and 2 m/s for $C = 1$ and $C = 5$, respectively.
- Solar irradiance has a negative influence on the output power of the unconcentrated STEG; however, it has a positive influence on the output power of the concentrated STEG. The radiative cooling power also increases linearly with solar irradiance for both concentrated and unconcentrated cases.

Although the concentrated STEG-RC has higher output performance compared to the unconcentrated case, long-term exposure to the sun may lower the output performance due to the low cooling performance of the radiative cooler. This limitation can be clearly seen in transient analysis, which is considered one of the future research directions of this study. It should also be noted that in practice, a single or dual-axis solar tracker is needed for the concentrated STEG-RC system, which means additional energy consumption for the system. Having said that, these two limitations are minimal for the unconcentrated STEG-RC system. Therefore, by integrating a heat sink with the radiative cooler, the output performance of the unconcentrated STEG-RC can be further enhanced.

Funding / Acknowledgement

This research is funded by the Scientific and Technological Research Council of Türkiye with Project number 123E144 and Scientific Research Unit of Istanbul University-Cerrahpaşa with Project number FBA-2023-37401.

REFERENCES

- [1] M. A. Zoui, S. Bentouba, D. Velauthapillai, N. Zioui, and M. Bourouis, "Design and characterization of a novel finned tubular thermoelectric generator for waste heat recovery", *Energy*, Aug., vol. 253, p. 124083, 2022.
- [2] D. Astrain, J. J. Fernandez, M. Araiz, A. Francone, L. Catalan, A. J. -Martín, P. Alegría, and C. M. S.-Torres, "Enhanced behaviour of a passive thermoelectric generator with phase change heat exchangers and radiative cooling", *Applied Thermal Engineering*, May, vol. 225, p. 120162, 2023.
- [3] A. Yusuf and S. Ballikaya, "Electrical, thermomechanical and cost analyses of a low-cost thermoelectric generator", *Energy*, Feb., vol. 241, p. 122934, 2022.
- [4] S. Qing, H. Yuan, C. Chen, S. Tang, X. Wen, J. Zhong, and X. Gou, "Characteristics and single/multi-objective optimization of thermoelectric generator by comprehensively considering inner-connection-and-contact effects and side-surface heat loss", *Energy Conversion and Management*, Jan., vol. 251, p. 115003, 2022.
- [5] T. Koshi, K. Okawa, Y. Amagai, N. Sakamoto, K. Nomura, and M. Yoshida, "High-performance stretchable thermoelectric generator using serpentine interconnects encapsulated in an ultrasoft silicone sponge", *Flex. Print. Electron.*, vol. 7, no. 2, p. 025008, 2022.
- [6] A. Yusuf, Y. Demirci, T. Maras, S. E. Moon, J. Pil-Im, J. H. Kim, and S. Ballikaya, "Experimental and Theoretical Investigation of the Effect of Filler Material on the Performance of Flexible and Rigid Thermoelectric Generators", *ACS Appl. Mater. Interfaces*, vol. 13, no. 51, pp. 61275–61285, 2021.
- [7] E. A. Bekele and V. R. Ancha, "Transient performance prediction of solar dish concentrator integrated with stirling and TEG for small scale irrigation system: A case of Ethiopia", *Heliyon*, vol. 8, no. 9, p. e10629, 2022.
- [8] X. Liu, P. Zhao, C.-Y. He, W.-M. Wang, B.-H. Liu, Z.-W. Lu, Y.-F. Wang, H.-X. Guo, G. Liu, and X.-H. Gao, "Enabling Highly Enhanced Solar Thermoelectric Generator Efficiency by a

- CuCrMnCoAlN-Based Spectrally Selective Absorber", *ACS Appl. Mater. Interfaces*, Vol. 14, no. 44, pp. 50180-50189, 2022.
- [9] Z. Su, D. Luo, R. Wang, Y. Li, Y. Yan, Z. Cheng, and J. Chen, "Evaluation of energy recovery potential of solar thermoelectric generators using a three-dimensional transient numerical model", *Energy*, Oct., vol. 256, p. 124667, 2022.
- [10] M. Alobaid, C. Maduabuchi, A. Albaker, A. Almalaq, M. Alanazi, and T. Alsuwian, "Machine learning and numerical simulations for electrical, thermodynamic, and mechanical assessment of modified solar thermoelectric generators", *Applied Thermal Engineering*, Feb., vol. 220, p. 119706, 2023.
- [11] A. Yusuf and S. Ballikaya, "Performance analysis of concentrated photovoltaic systems using thermoelectric module with phase change material", *Journal of Energy Storage*, Mar., vol. 59, p. 106544, 2023.
- [12] K. Karthick, S. Suresh, M. M. M. D. Hussain, H. M. Ali, and C. S. S. Kumar, "Evaluation of solar thermal system configurations for thermoelectric generator applications: A critical review", *Solar Energy*, Aug., vol. 188, pp. 111-142, 2019.
- [13] H. Jo, Y. Joo, and D. Kim, "Thermal design of solar thermoelectric generator with phase change material for timely and efficient power generation", *Energy*, Jan., vol. 263, p. 125604, 2023.
- [14] J. Ko, S.-Y. Cheon, Y.-K. Kang, and J.-W. Jeong, "Design of a thermoelectric generator-assisted energy harvesting block considering melting temperature of phase change materials", *Renewable Energy*, Jun., vol. 193, pp. 89-112, 2022.
- [15] Z. Xia, Z. Zhang, Z. Meng, and Z. Yu, "A 24-hour thermoelectric generator simultaneous using solar heat energy and space cold energy", *Journal of Quantitative Spectroscopy and Radiative Transfer*, Aug., vol. 251, p. 107038, 2020.
- [16] H. Pan and D. Zhao, "An improved model for performance predicting and optimization of wearable thermoelectric generators with radiative cooling", *Energy Conversion and Management*, May, vol. 284, p. 116981, 2023.
- [17] J. Guo and X. Huai, "Maximizing Electric Power through Spectral-Splitting Photovoltaic-Thermoelectric Hybrid System Integrated with Radiative Cooling", *Advanced Science*, vol. 10, no. 10, p. 2206575, 2023.
- [18] D. Zhao, A. Aili, Y. Zhai, S. Xu, G. Tan, X. Yin, and R. Yang, "Radiative sky cooling: Fundamental principles, materials, and applications", *Applied Physics Reviews*, vol. 6, no. 2, p. 021306, 2019.
- [19] L. Zhou, H. Song, N. Zhang, J. Rada, M. Singer, H. Zhang, B. S. Ooi, Z. Yu, and Q. Gan, "Hybrid concentrated radiative cooling and solar heating in a single system", *Cell Reports Physical Science*, vol. 2, no. 2, p. 100338, 2021.
- [20] J. Liu, Y. Zhang, D. Zhang, S. Jiao, Z. Zhang, and Z. Zhou, "Model development and performance evaluation of thermoelectric generator with radiative cooling heat sink", *Energy Conversion and Management*, Jul., vol. 216, p. 112923, 2020.
- [21] D. Zhao, A. Aili, Y. Zhai, J. Lu, D. Kidd, G. Tan, X. Yin, and R. Yang, "Subambient Cooling of Water: Toward Real-World Applications of Daytime Radiative Cooling", *Joule*, vol. 3, no. 1, pp. 111-123, 2019.
- [22] Y. Ji and S. Lv, "Experimental and numerical investigation on a radiative cooling driving thermoelectric generator system", *Energy*, Apr., vol. 268, p. 126734, 2023.
- [23] C.-H. Wang, H. Chen, Z.-Y. Jiang, and X.-X. Zhang, "Design and experimental validation of an all-day passive thermoelectric system via radiative cooling and greenhouse effects", *Energy*, Jan., vol. 263, p. 125735, 2023.
- [24] P. Berdahl and R. Fromberg, "The thermal radiance of clear skies," *Solar Energy*, vol. 29, no. 4, pp. 299-314, 1982.

- [25] H. Bao, C. Yan, B. Wang, X. Fang, C. Y. Zhao, and X. Ruan, "Double-layer nanoparticle-based coatings for efficient terrestrial radiative cooling", *Solar Energy Materials and Solar Cells*, Aug., vol. 168, pp. 78–84, 2017.
- [26] D. Jiang, Z. Fan, M. Dong, Y. Shang, X. Liu, G. Chen, and S. Li, "Titanium nitride selective absorber enhanced solar thermoelectric generator (SA-STEG)", *Applied Thermal Engineering*, Aug., vol. 141, pp. 828–834, 2018.
- [27] C. Maduabuchi, C. Eneh, A. A. Alrobaian, and M. Alkhedher, "Deep neural networks for quick and precise geometry optimization of segmented thermoelectric generators", *Energy*, Jan., vol. 263, p. 125889, 2023.
- [28] Amazon, "SP1848-27145-Thermoelectric-Generator," 2023. [Online]. Available: <https://www.amazon.com/SP1848-27145-Thermoelectric-Generator-Temperature-Generation/dp/B07J54H41F>. [Accessed August 22, 2023].
- [29] Robotistan, "Solarx güneş takip sistemi - 2. nesil," 2023. [Online]. Available: <https://www.robotistan.com/solarx-gunes-takip-sistemi-elektronikli>. [Accessed September 20, 2023].
- [30] Ferrotec, "Reliability of thermoelectric cooling module," 2023. [Online]. Available: <https://thermal.ferrotec.com/technology/thermoelectric-reference-guide/thermalref10/> [Accessed September 20, 2023].